TEXTURE ANALYSIS OF TISSUE AGING USING GLOBAL AND CLUSTER CONSTRAINED LOCAL CODING

Yang Song[1], *Weidong Cai*[1], *Heng Huang*[2], *David Dagan Feng*[1], *Yue Wang*[3], *Mei Chen*[4,5]

[1]BMIT Research Group, School of IT, University of Sydney, Australia
[2]Department of Computer Science and Engineering, University of Texas, Arlington, USA
[3]Bradley Department of Electrical and Computer Engineering, Virginia Tech, USA
[4]Computer Engineering Department, University of Albany State University of New York, USA
[5]Robotics Institute, Carnegie Mellon University, USA

ABSTRACT

Morphological age of various tissues provides important information about aging processes. In this paper, we propose a method for quantifying the tissue age of pharynx terminal bulb in *C.elegans* from microscopy images. Our method comprises two main components: (i) a multi-modal texture descriptor extracted at two scales; and (ii) an age quantification algorithm with global and cluster-constrained local coding. The performance of our proposed method is evaluated on 970 images of seven age classes in the publicly available IICBU dataset. Our method achieves 21% improvement in classification accuracy when compared to that of the benchmark platform, and our local coding algorithm outperformed the support vector machine model by 10%.

Index Terms— Texture analysis, local coding, classification, microscopy imaging.

1. INTRODUCTION

As a prevalent biological process in nature, aging affects all of the body's cells and tissues, and causes loss of functions. Understanding the aging process is critical to improving our quality of life. However, aging is a complex process with different effects on different organs and different people, and these complexities hinder the progress of aging studies [1]. One of the challenging tasks is the quantification of morphological age of tissues from microscopy image based on the tissue morphology. Tissues of the same chronological age could exhibit different morphological characteristics due to individual differences. The morphological age thus provides more insight into the physiological characteristics of tissue aging compared to the chronological age [2]. However, manual analysis of microscopy images is subject to individual bias and limited by the capability of human eyes. It is thus desirable to develop a computerized system to support more objective and consistent analysis of tissue ages.

This work was supported in part by ARC grants.

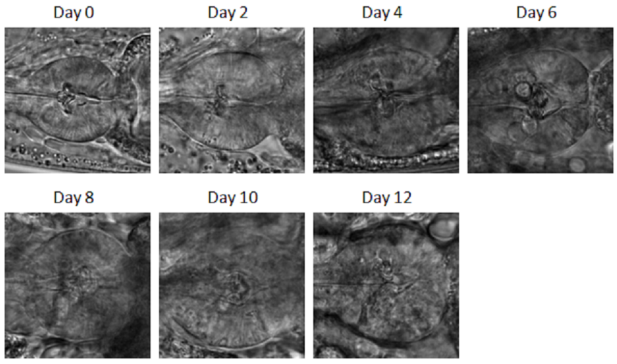

Fig. 1: Sample terminal bulb images of seven chronological ages from the IICBU dataset.

The *C.elegans* is a valuable experimental organism in aging studies since its tissue aging can be analyzed using a microscope during its short lifespan of 2–3 weeks. In particular, the pharynx terminal bulb of *C.elegans* is often used, and structural deterioration of muscle tissues can be observed as the terminal bulb ages [3] (Fig. 1). To support computerized aging quantification, texture entropy has been reported as a good indicator of the morphological ages [2].

On the other hand, it is difficult to evaluate objectively the accuracy of the quantified morphological age, since it is a continuous number and subjective when determined manually. However, tissues of different chronological ages normally have separate ranges of morphological ages, hence one way of quantitative evaluation is to quantize the morphological ages into discrete chronological ages and measure the classification accuracy of chronological ages. A number of studies have attempted to perform such classification on the terminal bulb images [4, 5, 6, 7, 8]. In these studies, the images are typically represented by a combination of texture features, such as the Haralick feature and speed-up robust features (SURF). Classification of tissue ages is then performed using the nearest neighbor classifier [4, 8], support vector ma-

chine (SVM) [5, 7], or subspace ensemble classifier [6].

In this study, we propose a new method to quantify the morphological age of terminal bulb tissues from differential interference contrast (DIC) microscopy images. Our methodological contributions are three-fold. First, we propose a different way of texture representation of the terminal bulb images with a highly discriminative multi-modal descriptor. Second, to quantify the tissue ages, we design a global and cluster-constrained local coding (GCLC) method, which provided large improvement in classification accuracy over SVM. Third, we evaluated our method on the publicly available IICBU dataset [9], and achieved 70.1% classification accuracy compared to 49% accuracy reported by the benchmark platform of this dataset [4]. Furthermore, we would like to mention that our GCLC method is highly efficient with the local coding construct, and can be generally applicable to other imaging problems with few parameters.

2. METHODS

2.1. Dataset

The terminal bulb aging dataset in the IICBU database contains 970 DIC microscopy images of 300×300 pixels. The images capture the pharynx terminal bulb region of *C.elegans*, and are collected at seven different ages: 0, 2, 4, 6, 8, 10, 12 days. The images are labeled into seven classes according to the chronological ages. The number of images belong to each class is: 106, 218, 159, 176, 195, 62 and 54. Sample images are shown in Fig. 1.

2.2. Texture Feature Extraction

It can be seen from Fig. 1 that the terminal bulb images are mainly characterized by textures. We thus propose to incorporate four types of texture descriptors: the local binary patterns (LBP) [10], histogram of oriented gradients (HOG) [11], GIST [12] and census transform histogram (CENTRIST) [13]. Our empirical study shows that these descriptors are much more effective than the other traditional texture features such as the gray-level co-occurrence matrix, wavelet and curvelet transforms.

The LBP/HOG/GIST descriptors are first extracted following the standard settings with 16 cells, resulting in descriptors of 16×58, 16×31 and 16×32 dimensions. The CENTRIST descriptor is computed for the whole image and is of 256 dimensions. Next, we note that more detailed texture changes between different ages can be observed at the central areas of the images compared to the border areas. Hence, we extract a square region of $1/4$ of the image size from the image center, and compute the 16-cell LBP/HOG descriptors from it at a finer scale. The overall multi-modal descriptor is the concatenation of all individual descriptors that are L2 normalized, and has a total dimension of $16 \times (58 + 31 + 32) + 256 + 16 \times (58 + 31) = 3616$.

2.3. Tissue Age Quantification

The aim of tissue age quantification is to compute a continuous number $s \in [0, 12]$ representing the morphological age of a terminal bulb image I. To do this, we design a sparse representation-based GCLC method with two levels of local coding. The method produces a difference vector d representing the distance of I from each chronological age, and s is then derived from d.

2.3.1. Global Scope Local Coding

We denote a test image by its descriptor $f \in \mathbb{R}^H$ and $H = 3616$ is the descriptor dimension. With global scope local coding, we derive a difference vector $d^G \in \mathbb{R}^7$, in which a lower element value indicating a closer match of f with the respective age class.

To do this, seven reference dictionaries are first constructed from the training data, with each dictionary $D_l \in \mathbb{R}^{H \times N_l}$ containing N_l descriptors from the age class $l \in \{1, .., 7\}$. We then adopt the locality-constrained linear coding (LLC) [14] algorithm to compute a local coding f_l of f based on the reference dictionary D_l:

$$f_l = D_l^f x_l \tag{1}$$

where $D_l^f \in \mathbb{R}^{H \times K}$ is the locally adaptive reference dictionary containing K descriptors (reference data) from D_l that are most similar to f (measured based on Euclidean distances). $x_l \in \mathbb{R}^K$ is a weight vector, and is derived by:

$$\min_{x_l} \|f - D_l^f x_l\|^2 + \lambda \|v \odot x_l\|^2, \;\; s.t. \; \mathbf{1}^T x_l = 1 \tag{2}$$

where $v \in \mathbb{R}^K$ contains the Euclidean distances between f and each descriptor in D_l^f, and λ is a constant parameter typically set as 0.01. The use of D_l^f instead of D_l ensures that only locally similar reference data are used to encode f_l, and $\|v \odot x_l\|^2$ encourages higher weights to be assigned to reference data that are more similar to f. LLC has an analytical solution and x_l is efficiently solved.

The local coding f_l can be considered as a sparse representation of f by class l. Based on this, we define the lth element of the difference vector d^G as:

$$d^G(l) = \|f - f_l\|_2. \tag{3}$$

If f_l closely matches f, i.e. a small $d^G(l)$, then it implies a high probability that f belongs to class l.

2.3.2. Cluster Constrained Local Coding

We note that the representativeness of d^G is largely affected by the selection of D_l^f. If f does not belong to class l but does appear highly similar to D_l^f, we could get a low difference in $d^G(l)$. Such cases often occur due to large inter-class

overlap and intra-class variation. We thus propose a cluster-constrained local coding method, in which the locally adaptive dictionary D_l^f is constructed based on feature space clustering rather than direct Euclidean distance computation.

Specifically, we first perform clustering on the entire dataset to partition the descriptors into M clusters using our locality-constrained subspace clustering (LSC) method [15]. This method incorporates the LLC model to compute an affinity matrix efficiently, based on which the spectral clustering is conducted to obtain the clusters. The descriptors that are in the training set and grouped into the same cluster as f are used as $\{D_l\}$. Then, from each D_l, $K/2$ descriptors that are most similar to f are used to construct the locally adaptive dictionary $D_l^f \in \mathbb{R}^{H\times K/2}$. This D_l^f is used in Eqs. (1) and (2) to derive the local coding f_l. Note that if the cluster does not contain training data of a certain class l, the corresponding D_l would be null, and then f_l is set to $\mathbf{0}$. Finally, a difference vector $d^C \in \mathbb{R}^7$ is computed similarly using Eq. (3).

2.3.3. *Probability-based Quantification*

Based on the local codings, the overall difference vector of test image f is computed as $d = \alpha d^G + d^C$, where α is a constant parameter. A vector $p \in \mathbb{R}^7$ is then computed to represent the probability of f belonging to each class with

$$p(l) = \exp\{10\,(1 - \frac{d(l)}{\sum_{l'=1}^{7} d(l')})\}. \quad (4)$$

Here the exponential operation with scale 10 is used to enlarge the differences between $p(l)$ of different classes.

Assume that the highest probability is obtained for class l. We then define the morphological age s of f as:

$$s = 2\theta - 2, \quad \theta = \frac{\sum_{l'=l-1}^{l+1} l' p(l')}{\sum_{l'=l-1}^{l+1} p(l')}. \quad (5)$$

Here $\theta \in [1, 7]$ is a continuous number produced by the average of three age classes ($l-1$, l and $l+1$) weighted by the probabilities of f belonging to each of them. $2\theta - 2$ then converts this number to an age value in the range of 0 to 12. Note that if $l = 1$, then l is used in place of $l-1$; and if $l = 7$, then l is used in place of $l+1$.

3. RESULTS

For training and testing, we applied five-fold cross validation. During each run, $4/5$ of the data were used for training and $1/5$ for testing. Our method contains three main parameters: the number of locally similar descriptors K, the number of clusters M, and the α factor used to compute d. Based on our empirical studies, we set these parameters to 40, 2 and 2, respectively.

Fig. 2 shows the histograms of the morphological ages derived for each chronological age. We expect the continuous morphological age to deviate from the discrete chronological age by a relatively small extent. The results show that for the first five age classes, the majority of images of each class obtain the same morphological age as indicated by the peaks of the curves, and the peaks are well separated between different chronological ages. Hence the majority of images of the first five age classes obtained meaningful morphological ages. However, the median ages of classes day 10 and day 12 are both 10.0 days, resulting in incorrect morphological ages of many images in class day 12. This is because that as the terminal bulb ages, the visual distinctions between different ages become more difficult to perceive, and this makes it more challenging to quantify the older ages.

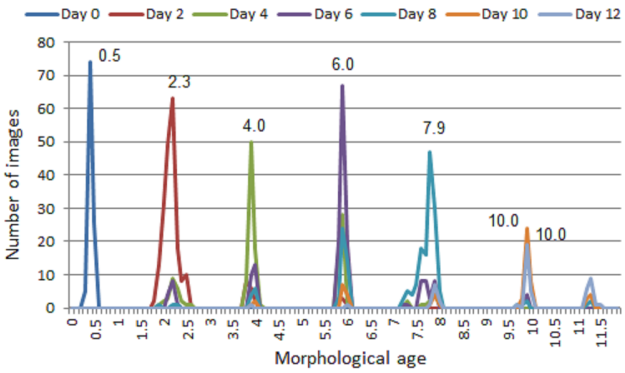

Fig. 2: Distribution of the morphological ages derived. The numbers above the curves indicate the median morphological ages obtained from images of each chronological age.

Table 1: Our classification accuracy (%) compared to SVM, WND-CHARM [4] and BIOCAT [7].

Ours	SVM	WND-CHARM	BIOCAT
70.1	60.0	49	51.1

For quantitative evaluation, we further classified the images into 7 age classes by assigning each image to the class with the highest $p(l)$. We compared our classification accuracy with (i) WND-CHARM [4], which is the benchmark platform of the IICBU database; (ii) BIOCAT [7], which is a more recent study on this database; and (iii) an SVM-based approach that uses the linear-kernel SVM with our proposed descriptor. The linear-kernel SVM was found more effective than the commonly used non-linear models. Table 1 shows that our method largely outperformed the compared approaches. Note that both WND-CHARM and BIOCAT use a combination of more traditional texture descriptors such as the wavelet features. BIOCAT uses the SVM classifier; and its lower performance compared to the evaluated SVM approach indicates the advantage of our proposed multi-modal descriptor. In addition, the confusion matrix in Fig. 3 shows that day 12 was the most difficult age to be classified, with a

	Day0	Day2	Day4	Day6	Day8	Day10	Day12
Day0	0.99	0.01	0.00	0.00	0.00	0.00	0.00
Day2	0.00	0.89	0.09	0.03	0.00	0.00	0.00
Day4	0.00	0.17	0.50	0.28	0.06	0.00	0.00
Day6	0.00	0.06	0.11	0.63	0.16	0.03	0.00
Day8	0.00	0.01	0.04	0.21	0.70	0.02	0.01
Day10	0.00	0.00	0.06	0.16	0.08	0.60	0.10
Day12	0.00	0.00	0.00	0.00	0.19	0.47	0.35

Fig. 3: Confusion matrix of the classification results.

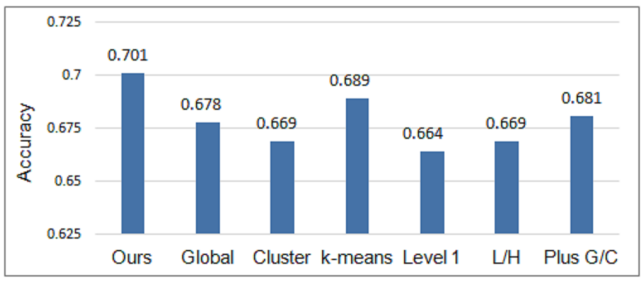

Fig. 4: Classification accuracy comparing our method with other variations of our method.

large portion of it misclassified as day 10.

To evaluate the effects of our method components, we experimented with the following variations of our method: (i) Global, which uses only the global scope local coding with the cluster-constrained local coding; (ii) Cluster, which uses only the cluster-constrained local coding; (iii) k-means, which uses the k-means method in place of LSC for generating the clusters used in cluster-constrained local coding; (iv) Level 1, which includes only the image-level descriptors without the LBP/HOG descriptors at the finer scale; (v) L/H, which includes LBP/HOG at both image-level and finer scale without the GIST/CENTRIST descriptors; and (vi) Plus G/C, which includes GIST/CENTRIST descriptors extracted at the finer scale in additional to our descriptor used.

Fig. 4 shows that our proposed method achieved the best classification accuracy. Our improvement over Global indicates the advantage of incorporating the cluster-constrained local coding. The lower accuracy using k-means suggests that the clustering performance for cluster-constrained local coding has a high impact on the classification accuracy. In addition, our performance improvement over Level 1 demonstrates the benefit of including the LBP/HOG features at the finer scale. It is also interesting to note that Plus G/C decreased the classification performance. Therefore, while a multi-modal descriptor helps to represent an image from complementary aspects, including too many features could reduce the discriminative power of features.

4. CONCLUSIONS

In this study, we propose a method to quantify the morphological ages of terminal bulb in *C.elegans* using DIC microscopy images. We designed a multi-modal texture feature based on general descriptors, and a global and cluster-constrained local coding method to quantify the tissue ages with sparse representation-based distance measures. We used the publicly available IICBU dataset for evaluation and obtained encouraging performance.

5. REFERENCES

[1] MedlinePlus U.S. National Library of Medicine, "Aging changes in organs - tissue - cells," 2015, https://www.nlm.nih.gov/medlineplus/ency/article/004012.htm.

[2] L. Shamir, C. A. Wolkow, and I. G. Goldberg, "Quantitative measurement of aging using image texture entropy," *Bioinformatics*, vol. 25, no. 23, pp. 3060–3063, 2009.

[3] J. Johnston, W. B. Iser, D. K. Chow, I. G. Goldberg, and C. A. Wolkow, "Quantitative image analysis reveals distinct structural transitions during aging in caenorhabditis elegans tissues," *PLos ONE*, vol. 3, no. 7, pp. e2821, 2008.

[4] L. Shamir, N. Orlov, D. M. Eckley, T. J. Macura, J. Johnston, and I. G. Goldberg, "Wndchrm - an open source utility for biological image analysis," *Source Code Biol. Med.*, vol. 3, no. 1, pp. 13, 2008.

[5] L. P. Coelho, J. D. Kangas, A. W. Naik, E. Osuna-Highley, E. Glory-Afshar, M. Fuhrman, R. Simha, P. B. Berget, J. W. Jarvik, and R. F. Murphy, "Determining the subcellular location of new proteins from microscope images using local features," *Bioinformatics*, vol. 29, no. 18, pp. 2343–2349, 2013.

[6] T. Meng and M. Shyu, "Biological image temporal stage classification via multi-layer model collaboration," *ISM*, pp. 30–37, 2013.

[7] J. Zhou, S. Lamichhane, G. Sterne, B. Ye, and H. Peng, "BIOCAT: a pattern recognition platform for customizable biological image classification and annotation," *BMC Bioinformatics*, vol. 14, pp. 291, 2013.

[8] T. D. Pham, "Classification of complex biological aging images using fuzzy kolmogorov-sinai entropy," *J. Phys. D: Appl. Phys.*, vol. 47, pp. 485402, 2014.

[9] L. Shamir, N. Orlov, D. M. Eckley, T. J. Macura, and I. G. Goldberg, "IICBU 2008: a proposed benchmark suite for biological image analysis," *Med. Biol. Eng. Comput.*, vol. 46, no. 9, pp. 943–947, 2008.

[10] T. Ojala, M. Pietikainen, and T. Maenpaa, "Multiresolution gray-scale and rotation invariant texture classification with local binary patterns," *IEEE Trans. Pattern Anal. Mach. Intell.*, vol. 24, no. 7, pp. 971–987, 2002.

[11] P. F. Felzenszwalb, R. B. Girshick, D. McAllester, and D. Ramanan, "Object detection with discriminatively trained part-based models," *IEEE Trans. Pattern Anal. Mach. Intell.*, vol. 32, no. 9, pp. 1627–1645, 2010.

[12] A. Oliva and A. Torralba, "Modeling the shape of the scene: a holistic representation of the spatial envelope," *International Journal of Computer Vision*, vol. 42, no. 3, pp. 145–175, 2001.

[13] J. Wu and J. M. Rehg, "CENTRIST: a visual descriptor for scene categorization," *IEEE Trans. Pattern Anal. Mach. Intell.*, vol. 33, no. 8, pp. 1489–1501, 2011.

[14] J. Wang, J. Yang, K. Yu, F. Lv, T. Huang, and Y. Gong, "Locality-constrained linear coding for image classification," *CVPR*, pp. 3360–3367, 2010.

[15] Y. Song, W. Cai, Q. Li, F. Zhang, D. Feng, and H. Huang, "Fusing subcategory probabilities for texture classification," *CVPR*, pp. 4409–4417, 2015.